Optimization of Interior Permanent Magnet Motor on Electric Vehicles to Reduce Vibration Caused by the Radial Force

L. Y. Xiang, S. G. Zuo, L. C. He, M. H. Zhang, J. J. Hu, and G. Long

Clean Energy Automotive Engineering Center
Tongji University, Shanghai 201804, China
xlongyang10@126.com, sgzuo@tongji.edu.cn, helvchang2006@163.com, zsyzmh@126.com,
ericaj@126.com, longguo.111@163.com

Abstract **–** The vibration and noise level of a driven motor on electric vehicles has a great influence on the overall comfort of the whole vehicle. In this paper, the main vibrational harmonic waves with high amplitudes of Interior Permanent Magnet (IPM) motor were investigated via an experiment. In order to lower the amplitudes of these harmonic waves, the paper carries out the optimization of radial force of the IPM motor based on the parameter sensitivity analysis and also implemented the structural optimization, according to the dynamic response of the stator. The final dynamic simulation of the optimized model excited by the optimized radial force, show that the optimization results in a better performance of the vibration behaviors. This study could provide some guidelines for the optimal design of the interior permanent magnet motor to reduce vibration.

Index Terms **–** Interior permanent magnet motor, radial force optimization, stator structural optimization and vibration behavior.

I. INTRODUCTION

An electric vehicle is one of the energy-saving and environmental-friendly transportation tools. The driven motor is one of the most important parts on an electric vehicle. However, the vibration and noise of the motors on vehicles is more serious than that of normal ones, which has a bad influence on the comfort of the vehicle. Thus it is necessary to conduct the study of the causes, factors and optimization of the vibration behaviors of the driven motors on electric vehicles. Interior Permanent Magnet (IPM) motors are most often used to drive the electric vehicles. For this kind of motor, the radial force inside stimulates the stator, which leads to the vibration and noise [1]. Accordingly, the existing studies on the vibration of IPM motors mainly focuses on the calculation and analysis of the radial force and the vibration modes of the stator.

Zhu is one of the earliest scholars to study the vibration and noise characteristics of permanent magnet motors. In his study, the instantaneous magnetic field distribution of brushless permanent magnet DC motor was calculated and the effects of four factors were analyzed: open-circuit field, armature-reaction field, stator slotting and loads. The results of analytical method agreed with the ones of finite element method [2]-[5], which laid the theoretical foundation of the calculation of the radial force; although, he didn't study the vibrational optimization of the motor. In the 21st century, the electromagnetic numerical method finite element method, as an example, is used more often for the motor analysis. Chen made use of finite element method to analyze the relationship between the radial force and stator teeth, width of rotor back iron and slot opening of the permanent magnet brushless motor. He found that the lower amplitudes of the radial forces resulted from larger stator teeth width, smaller rotor back iron width and slot opening [6]; however, he only pointed out the relationship and didn't further study the parameter optimization. Zhang studied the radial force of switched reluctance motors using skewed slot structure based on finite element method. The simulated results show that using skewed slot could reduce the radial force [7]; however, he didn't consider the effects of other parameters on the radial force, such as air gap length, thickness and depth of

Submitted On: April 17, 2013
Accepted On: March 11, 2014

permanent magnet. Abbas used analytical and FEM to calculate the radial forces exerted on different parts of the coils [8]; however, he didn't consider the effects of the radial force on the vibration of the motor.

In addition, there were also some scholars who studied the structural optimization of motor stators. Choi presented a topology optimization method of IPM motor stator cores to reduce cogging torque. The optimization results show that configurations having dummy slots were desirable, but the number of dummy slots differed [9]. Kwack used the level set method to optimize the structure of motor stator in order to reduce torque ripples, by minimizing the difference between torque values at defined rotor positions and the constant target torque value under constrained material usage [10]. Both studied the torque, instead of the vibration of the motors. Additionally, they didn't use a 3-D model for the optimization.

This paper aims at the vibration reduction of IPM motor by the optimization of radial force and stator structure, which are the two main factors of motor vibration. It discusses the vibration behavior of IPM motor on electric vehicles via an experiment to investigate the main vibrational harmonic waves with high amplitudes. Then the parameters that have influences on the radial forces were optimized according to the sensitivity analysis, as well as the 3-dimentinal model of stator was optimized to reduce the dynamic response of the stator. Lastly, the final simulation of the optimized stator model excited by the optimized radial forces showed that the vibration level of the stator had declined to a large extent than that of the original model, which meant that the vibration behavior of the IPM stator was much better.

II. EXPERIMENTAL ANALYSIS

In this paper, in order to measure the vibration level of the IPM motor a test bench was established, which can take into account the effects of changing loads of torques. The noise was also measured; although, in this experiment we mainly focus on the vibration analysis.

A. Experiment introduction

In this paper, a test bench system was established to measure the vibration of the IPM motor used to drive electric vehicles, as shown in Fig. 1. The system included electric eddy current dynamometer, its controller and cooling water box as the loading subsystem, as well as the protective cover and sound absorption material as the sound isolating subsystem. Nine microphones were arranged around the motor, as shown in Fig. 2 (a) (black points); there were also 4 vibration acceleration transducers pasted on the surface of the motor, as shown in Fig. 2(b).

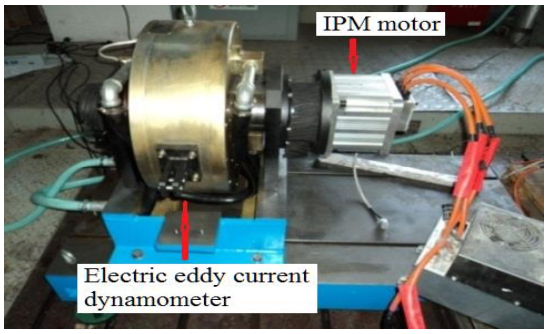

Fig. 1. Vibration test bench of IPM motor.

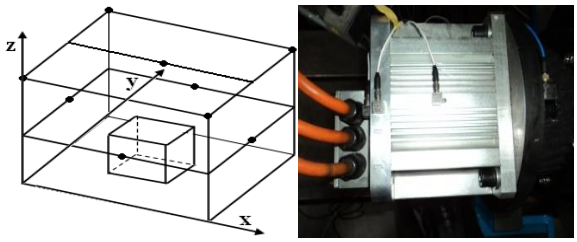

(a) (b)

Fig. 2. Arrangement of microphones and vibration acceleration transducers.

In order to study the real vibration levels of the IPM motor on an electric vehicle, the working conditions of the testing motor should be the same as those working on electric vehicles. The working conditions of the motor in this experiment included steady ones and transient ones. The steady states of the motor corresponded to those when the vehicle drove with the velocity from 5 Km/h to 40 Km/h; every 5 Km/h as an increment. The transient conditions of the motor corresponded to those when the vehicle sped up with the velocity from 5 Km/h to 40 Km/h. The correspondent rotational speeds and torques were calculated according to the vehicles driving conditions. In this way, the vibration levels of the motor on the test bench were almost the same as on the electric vehicle.

B. Vibration analysis of experimental results

In order to study the relationship of the vibration level and the rotational speed of the motor, the paper carried out the frequency spectrum analysis of the vibration acceleration signals of the motor surface while the motor sped up. The waterfall of motor radial vibration acceleration is shown in Fig. 3.

It could be found from Fig. 3 that there were vibration harmonic waves that changed with the rotational speed; because the law is the same for any rotational speed, it was reasonable to choose one steady state of the motor for analysis to study the harmonic waves of the vibration spectrum. In addition, the rated condition was most often used and was representative; therefore, this paper chose the rated condition for study. The rotational speed was $n=2400r/\min$ and the torque was $T=30N/m$. The radial vibration frequency spectrum of the motor under this condition is shown in Fig. 4.

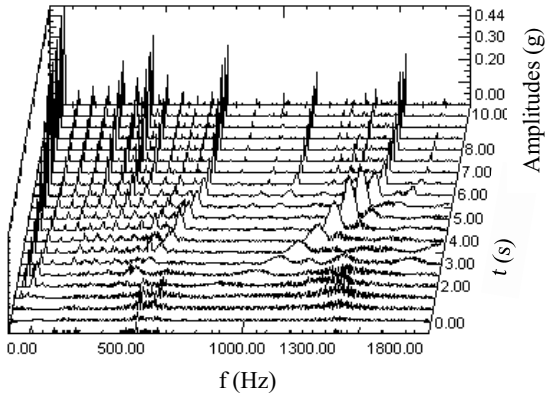

Fig. 3. Waterfall of motor radial vibration acceleration.

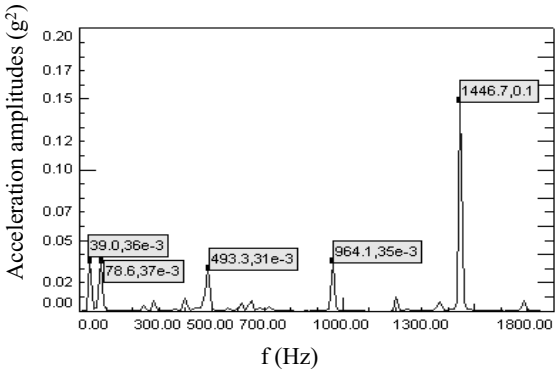

Fig. 4. Frequency spectrum of motor radial vibration acceleration.

For this working condition, the rotational frequency of the motor was $f=n/60=40Hz$. The frequency of controlling current was $f_1=n\cdot p/60=240Hz$; where $p=6$ was the number of pole-pairs of the motor. It was shown in Fig. 4 that the main components of motor vibration included the rotational frequency and its second harmonic frequency as well as the second, fourth, and sixth harmonic frequencies of the current frequency; where the sixth harmonic frequency has the highest amplitude.

As the rotational frequency and its second harmonic frequency were caused by the mechanical effects, this paper mainly studied the second, fourth and sixth harmonic waves of the current frequency of the vibration for optimization. Since the vibration of the IPM motor stator is mainly determined by the radial force and the stator structure, this paper implemented the optimization of the radial force and the stator structure, respectively in the following parts.

III. OPTIMIZATION OF RADIAL FORCE

A. Analytical calculation of radial force

According to Maxwell's law, the radial force was expressed as:

$$p_n(\theta,t)=\frac{b^2(\theta,t)}{2\mu_0}, \quad (1)$$

where μ_0 was the magnetic conductivity of air, $\mu_0=4\pi\times10^{-7}H/m$ and $b(\theta,t)$ was air gap magnetic flux density.

The air gap magnetic flux density could be calculated by:

$$b(\theta,t)=\lambda(\theta,t)f(\theta,t), \quad (2)$$

where $\lambda(\theta,t)$ was the air gap magnetic permeance and $f(\theta,t)$ was the air gap magnetic potential.

The air gap magnetic permeance was composed by 4 parts, as in:

$$\lambda(\theta,t)=\Lambda_0+\sum_{k1}\lambda_{k1}+\sum_{k2}\lambda_{k2}+\sum_{k1}\sum_{k2}\lambda_{k1}\lambda_{k2}, \quad (3)$$

where Λ_0 was the constant component, λ_{k1} was the harmonic wave magnetic permeance when the rotor was smooth and the stator was slotted and λ_{k2} was the harmonic wave magnetic permeance when the stator was smooth and the rotor was slotted.

The air gap magnetic potential was caused mainly by stator field current and rotor permanent

magnet, as in:

$$f_c = \frac{N_c I_c}{2}, \quad (4)$$

$$f_m(\theta,t) = f_0(\theta,t) + \sum_v f_v(\theta,t) + \sum_\mu f_\mu(\theta,t), \quad (5)$$

$$f(\theta,t) = f_c + f_m(\theta,t), \quad (6)$$

where f_c was the air gap magnetic potential caused by stator field current, N_c was the number of coil in one slot, I_c was the current in one coil, $f_m(\theta,t)$ was the air gap magnetic potential caused by rotor permanent magnet, $f_0(\theta,t)$ was the synthetic magnetic potential of fundamental wave, $f_v(\theta,t)$ was the harmonic wave magnetic potential of stator winding and $f_\mu(\theta,t)$ was the harmonic wave magnetic potential of rotor.

As for the real motor in this paper, the rotor was smooth, the stator was slotted and there was no air gap permeance. Leaving out the vibration force waves of high orders and low amplitudes, the radial force was expressed as:

$$p_n(\theta,t) = \frac{1}{2\mu_0}\left\{\frac{B_1^2}{2}\cos(2p\theta - 2\omega_1 t - 2\varphi_0) + \sum_v\sum_\mu B_v B_\mu \cos[(\mu \pm v)\theta - (\omega_\mu \pm \omega_1)t - (\varphi_\mu \pm \varphi_v)]\right\}. \quad (7)$$

In this formula, B_1 is the magnetic potential of the basic wave, p is the number of pole-pairs of the motor, θ is the angular displacement in the air gap, t is the time, μ, v are the orders of the harmonic waves, ω is the angular frequency of the harmonic wave and φ is the phase of the harmonic wave.

Similar with the working condition in the experiment, the radial force of the rated condition was calculated and the frequency spectrum is shown in Fig. 5.

Figure 5 shows that the main components of radial force included 480 Hz, 960 Hz and 1439 Hz, which are in accordance with the vibration frequency components measured in the experiment. They were respectively the second, fourth and sixth harmonic frequencies of the current frequency. Accordingly, the analytical calculation could reflect the harmonic waves of the radial force.

B. Magnetic finite element simulation

Magnetic finite element modeling:

For the 3-phase, 6-state IPM permanent motor with 18 teeth and 12 poles that was studied in this paper, the number of slots per pole per phase is 1/2. It was equal to 6 unit motors and each unit motor had 3 teeth and 2 poles. Since every unit motor had the same magnetic field, this paper used unit motors for magnetic simulation to save time. According to the real parameters of the motor, the magnetic model of 2 unit motors was established in ANSOFT. Then the stator, rotor, air gap and magnets were meshed with different sizes. After meshing of the model, the paper got the finite element model of the unit motors, as shown in Fig. 6.

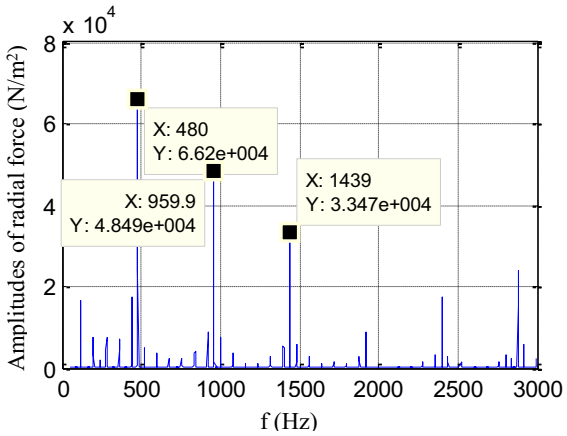

Fig. 5. Frequency spectrum of radial force in analytical method.

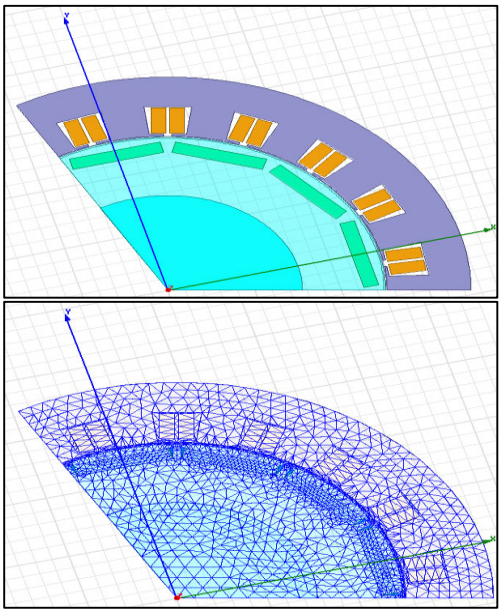

Fig. 6. Magnetic model and finite element model of the unit motors.

Calculation of radial force:

Under the rated working condition, the

rotating speed was 2400 r/min, the load was 18 N/m, the voltage was 120 v and the electric current frequency was 240 Hz. The Maxwell 2-D transient magnetic field solver was used for the simulation. The simulation step was 0.0001 s and the time duration was 0.5 s. For the finite element model of the unit motors under rated condition, the radial force in the air gap was calculated and its frequency spectrum is shown in Fig. 7.

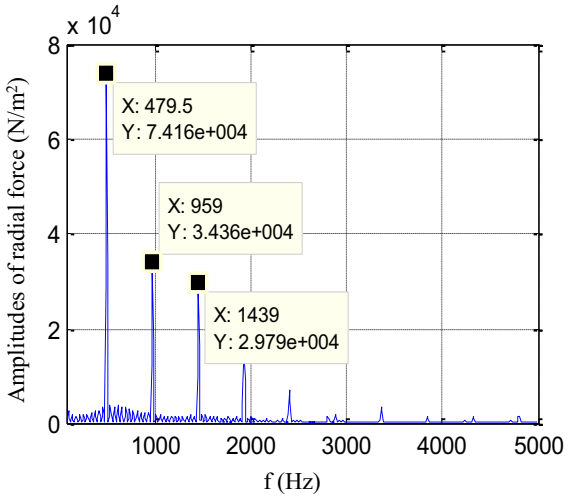

Fig. 7. Frequency spectrum of radial force in the air gap by simulation.

It was shown in Fig. 7 that the main frequencies of the radial force were the second, fourth and sixth harmonic frequencies of the current frequency. The results were in accordance with the main frequencies of analytical calculation, as in Fig. 5 and the experimental result, which confirmed the validity of the simulation. It was shown in both Figs. 5 and 7 that the energy of the second harmonic waves was more than 40% of the whole energy; the fourth and sixth harmonic waves were respectively about 20%. This means that the energy distribution and the ratio of harmonic waves were consistent. Considering that in the analytical calculation the equation (2) is an approximation, there is some deviation of the amplitudes between the analytical results and the simulation result. Therefore, the paper used the finite element model, which was more accurate than analytical model, for further analysis.

It was known from the experiment that the sixth harmonic wave of the current of the vibration had the highest amplitude, so the reduction of the amplitude of this wave in the radial force is the key for the improvement of the vibration behavior.

C. Parameter sensitivity analysis

It was obvious that the thickness and depth of the permanent magnet of IPM motor had an influence on the air gap flux density, which had an effect on the radial force. Additionally, the existing studies showed that the air gap length and the slot opening width also had an influence on the air gap flux density, which then affected the frequency and amplitude of the radial force [11]-[12]. This section used these four parameters for sensitivity analysis of the radial force under rated condition in order to choose the sensitive parameter intervals for optimization to get lower radial forces. Only one parameter changed at one time, the other settings remained unchanged. It should be noticed that the parameter ranges in this section all meet the requirement of design handbook of permanent magnetic motor, which means that the variations won't affect the performances of the motor too much [1].

The previous study in this paper showed that second, fourth and sixth harmonic waves of the radial force was the main exciting source of the vibration of the motor; therefore, this section mainly studied the parameter sensitivity to the second, fourth and sixth harmonic waves of radial force. During the study of the influence on the radial force of one parameter, other parameters remained unchanged. The studied ranges of the objective parameters were around and symmetrical about the original values of the motor. As the values were quite small, it is difficult and costly to manufacture extremely precise motors. Thus, it is not necessary to conduct a statistical study. The paper divided each parameter range into four intervals and four analysis, as shown in Table 1. Then when the value of the studied parameter is respective to the boundary values of the intervals, the second, fourth and sixth harmonic frequencies of the radial force are calculated. The results of the radial forces when the four parameters differed, are shown in Fig. 8. The comparison of the results indicated the laws that the radial force increased slowly with the increase of the width of stator slot openings, decreased slowly with the increase air gap length, increased rapidly with the increase of thickness of the permanent and decreased rapidly with the increase of depth of the permanent.

Table 1: Parameter intervals division

Parameters (mm)	Interval 1	Interval 2	Interval 3	Interval 4	Original Value
Slot opening width	(0.5, 1.5)	(1.5, 2.5)	(2.5, 3.5)	(3.5, 4.5)	2.5
Air gap length	(0.7, 0.8)	(0.8, 0.9)	(0.9, 1.0)	(1.0, 1.1)	0.9
Thickness of permanent magnet	(2.5, 3.5)	(3.5, 4.5)	(4.5, 5.5)	(5.5, 6.5)	4.5
Depth of permanent magnet	(0.1, 0.7)	(0.7, 1.3)	(1.3, 2.3)	(2.3, 3.3)	1.3

As the value of these four parameters differed so much, this paper used the following method to carry out the sensitivity analysis. Take the air gap length for example, the original air gap length was l_0 and the amplitude of sixth harmonic wave of the radial force was b_0. One interval of the air gap length was $l_1 \sim l_2$, when the air gap length was respectively l_1 and l_2, the corresponding amplitudes of sixth harmonic waves of the radial forces were b_1 and b_2. Then the change rate of air gap length in this interval was k_b, which was taken as the sensitivity index [13], was defined as:

$$k_b = \left[(b_2 - b_1)/b_0\right] / \left[(l_2 - l_1)/l_0\right].$$

It could be seen that k_b was a dimensionless quantity. It considered the original dimensions and the change at the same time so it could scientifically reflect the parameter sensitivity to radial force.

The change rates of other parameters were calculated in the same way with air gap length. The sensitivities of the four parameters in all intervals to the second, fourth and sixth harmonic waves are shown in Fig. 9. In Fig. 9, the positive and negative values meant that the amplitudes of radial force increased or decreased with the increase of the studied parameter.

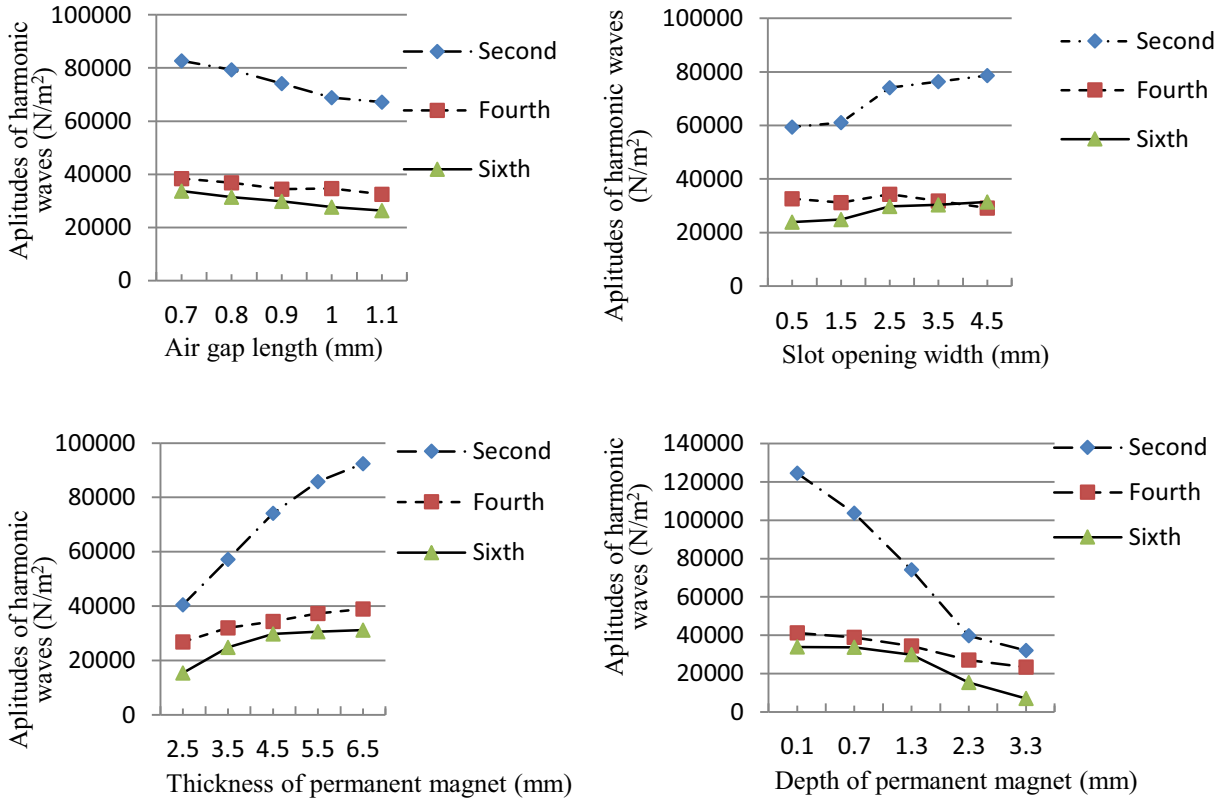

Fig. 8. Calculated radial forces of different parameters.

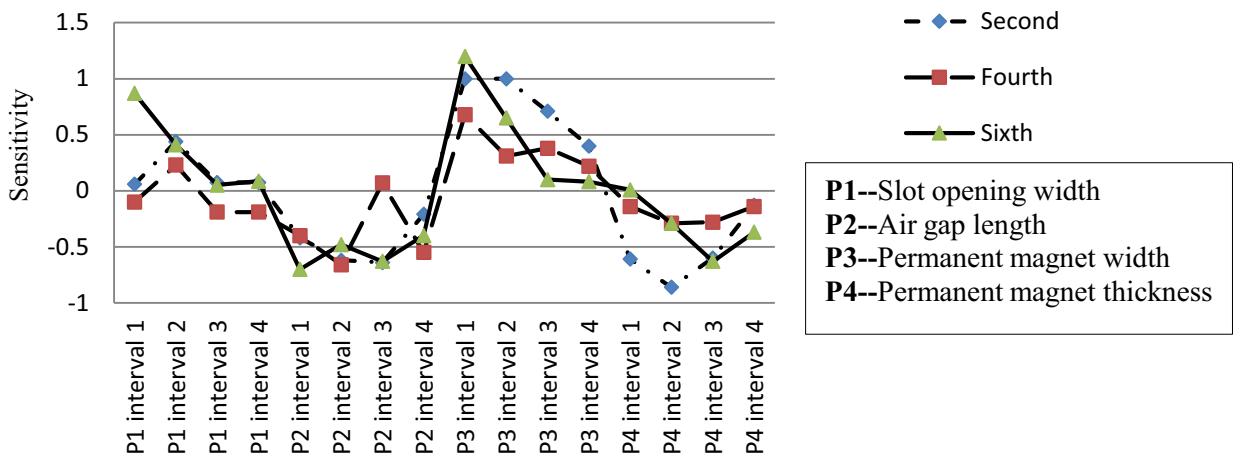

Fig. 9. Parameter sensitivities to the amplitudes of harmonic waves of radial force.

D. Parameter optimization

It was known from the previous analysis that it was important to reduce the amplitudes of the sixth harmonic waves of radial forces to reduce vibration. Those parameter intervals with high sensitivities to the sixth harmonic waves were interval 1 of width of permanent magnet, interval 3 of depth of permanent magnet, interval 1 and interval 2 of the width of stator slot opening, and all the intervals of the air gap length. Thus, the parameter values should be determined in these intervals respectively.

The paper determined the parameter values in order to achieve lower amplitudes of the radial forces according to what is analyzed above. The parameters should be chosen in the sensitive intervals and could result in smaller radial forces. In this way, the desired radial forces could be achieved without changing the parameters too much. Accordingly, the width of permanent magnet should be as small as possible in interval 1, the depth of permanent magnet should be as large as possible in interval 3 and the air gap length should be as large as possible in the four intervals. As for the stator slot opening width, the values in interval 1 were too small, which might lead to some errors and high costs of manufacture and installation. Also, with consideration of the sensitivity of the second and fourth harmonic waves, the value of slot opening width should be as small as possible in interval 2. Under the comprehensive consideration, the finally determined values of the parameters were shown in Table 2.

Table 2: Optimized parameter values

Parameters	Values (mm）
Thickness of permanent magnet	2.5
Depth of permanent magnet	2.3
Air gap length	1.1
Slot opening width	1.5

According to the optimized parameters in Table 2, the new finite element model of unit motors was established in software ANSOFT, to calculate the radial forces. The main frequencies of the radial force after optimization were the second, fourth and sixth harmonic frequencies of the current frequency; which were the same with those before optimization, but the amplitudes of the radial forces are optimized. The comparison of amplitudes of radial forces before and after optimization are shown in Table 3. It can be seen that the amplitudes of second, fourth and sixth harmonic waves had been reduced to a large extent; especially the amplitude of sixth harmonic wave, which declined by two-thirds.

IV. STATOR STRUCTURAL OPTIMIZATION

The purpose of the stator structural optimization in this paper was that when the weight and boundary dimension remained unchanged, the dynamic displacement responsecaused by the given excitation should be as small as possible. That is to say, when the excitation remains unchanged, the vibrational

energy of the stator should be reduced to improve the vibration behavior of the motor.

Table 3: Force amplitudes of main harmonic waves

Harmonic Waves	Second	Fourth	Sixth
Original amplitude (mm)	74160	34360	29790
Optimized amplitude (mm)	39870	21990	9967
Optimized percentage	46%	36%	67%

A. Determination of parameters and objective function for optimization

This chapter carried out the stator structural optimization of IPM motor on electric vehicles. The study aimed to improve the dynamic response behavior of the stator without changing the performance of the motor. During the design of motors, inner diameter and effective length of the iron core were the main parameters that determined the performance of the motor. The original values of the motor structural parameters are shown in Table 4.

Table 4: Motor parameter values

Parameters	Values
No. of pole-pairs	2p = 6
Inner diameter of iron core	$D_{i1} = 130\,mm$
Outer diameter of iron core	$D_1 = 180\,mm$
Shell thickness	$\Delta h = 4mm$
Yoke thickness	14 mm
Length of iron core	86 mm

The existing study indicated that the parameters that had an influence on the vibration modes of motor stator were the shell thickness, outer diameter of iron core and thickness of stator yoke [14]. As the yoke thickness was associated with the inner and outer diameters of the stator, when the inner diameter remains unchanged, the yoke thickness changes with the outer diameter. Thus, this paper chose the outer diameter of iron core and shell thickness as optimization variables. During the optimization, the unchanged inner diameter and effective length of the iron core ensured the performance of the motor.

The original value of shell thickness was 4 mm, which was quite small. With consideration of the requirement of structural strength, the range of shell thickness for optimization should be a little larger, as 4~8 mm in this paper. In addition, the volume of the motor shouldn't be too large, so the stator boundary dimension was set as less than 5% larger than the original value. At the same time, the minimum of the stator yoke thickness was set as 5 mm to avoid the magnetic saturation. Accordingly, the range of outer diameter of the iron core was 81~90 mm.

The optimization was achieved in software ANSYS and the whole process was conducted with ANSYS Parameter Design Language. The range between the maximum and the minimum of the dynamic displacement that was the fluctuating amplitude of the dynamic displacement of the stator surface, reflected the vibration energy of the stator. In order to reduce the vibration level of the motor stator, it was effective to reduce the fluctuating amplitude of the dynamic displacement of the stator surface, which was chosen as the objective function for optimization in this paper.

Accordingly, the parameters were set as follows during the optimization:

(1) Design variables:
Outer radius of the iron core: 81~90 mm;
Shell thickness: 4~8 mm.

(2) State variables:
$R_1 - R_{i1} \geq 16mm$ (stator yoke thickness is not smaller than 5 mm)
Stator boundary dimension $\leq$ 1.05×190 mm (original value)

(3) Objective function:
Fluctuating amplitude of dynamic displacement of the stator surface.

B. Optimization result

The process was programmed with ANSYS Parameter Design Language. First, the 3-D model of stator was established, as shown in Fig. 10. Second, the model was excited by the time-domain radial forces calculated by simulation in chapter 3.2.2. Then the transient analysis started. During the calculation, the shell thickness and outer radius of the iron core of the model changed to another set of values, according to equal step sweeping method of ANSYS and another step of transient analysis began. During every step, the objective function was recorded and it changed with the step number of the optimization, as shown in Fig. 11. Figure 11 showed that the objective function of the 26th step

number was the smallest, which meant the corresponding parameters were approximately the best. Then these parameters were rounded off, as shown in Table 5.

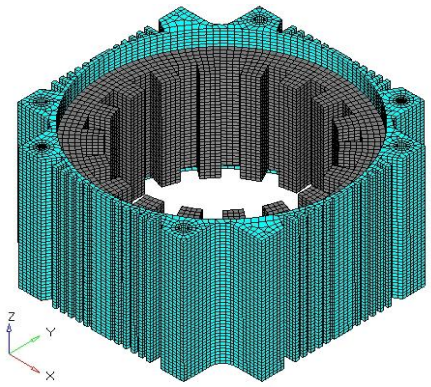

Fig. 10. Finite element model of the stator.

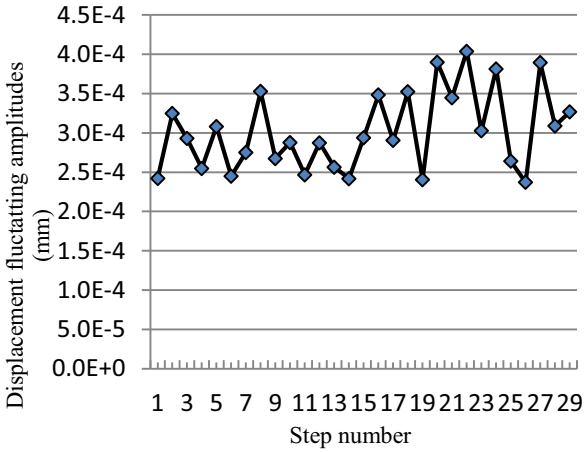

Fig. 11. Changes of objective function during optimization.

It was shown that after optimization the stator boundary dimension was only 2 mm larger than the original value, which met the requirement that it was less than 5% larger than the original value. Additionally, the outer diameter of the iron core decreased by 4 mm and the shell thickness increased by 4 mm. The transient displacement responses of the stator surface before and after optimization with the same excitation are shown in Fig. 12. The corresponding amplitudes of the main frequencies are shown in Table 6. In Table 6 it shows that after optimization the amplitudes of the main frequencies decreased to quite a large extent. That means that the dynamic response of the motor stator with the same excitation reduced after optimization.

Table 5: Parameters of motor stator after optimization

Parameters	Boundary Dimension	Outer Diameter of Iron Core	Shell Thickness
Values (mm)	192	176	8

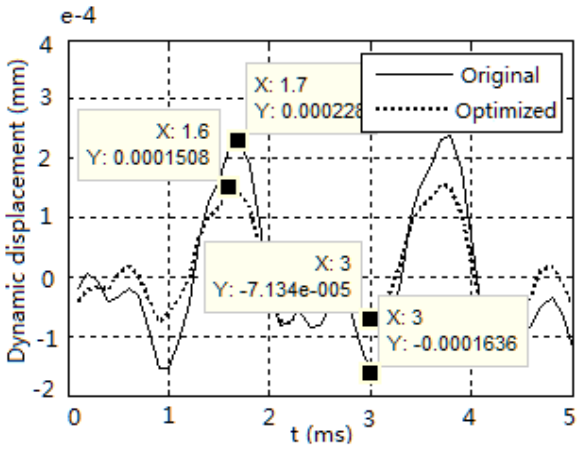

Fig. 12. Transient dynamic displacement responses of the stator before and after optimization.

Table 6: Displacement amplitudes of the main frequencies before and after optimization

Harmonic Frequencies	Second (480Hz)	Fourth (960Hz)	Sixth (1440Hz)
Original amplitude (mm)	6.69e-5	2.83e-5	5.12e-5
Optimized amplitude (mm)	3.85e-5	2.04e-5	3.68e-5
Percentage of optimization	42%	28%	28%

V. TRANSIENT DYNAMIC ANALYSIS OF THE OPTIMIZED MODEL

After the optimization of the radial force and the stator structure, a new model was established for simulation to verify the optimization effect. The optimized finite element model of the stator was excited by the optimized radial force for frequency response analysis.

Then the paper conducted the frequency

response analysis of the rated condition, which was a steady state. The results of the frequency response analysis showed that after optimization the main harmonic frequencies of the vibration acceleration were the same with those before optimization. They were 480 Hz, 960 Hz and 1439 Hz, which were the second, fourth and sixth harmonic frequencies of the current frequency; especially the sixth harmonic wave with the highest amplitude. The amplitudes of the main harmonic waves decreased to a large extent. The comparison of the amplitudes of the harmonic waves are shown in Table 7. It could be found from Table 7 that the average decrease of the amplitudes was 60%, which meant the optimization reduced the vibration level greatly. Accordingly, the optimization was quite ideal.

Table 7: Vibration acceleration amplitudes of main frequencies

Frequency (Hz)	480	960	1439
Original amplitudes (m/s^2)	0.7	0.6	1.9
Optimized amplitudes (m/s^2)	0.17	0.20	1.0
Percentage of optimization	76%	67%	37%

VI. CONCLUSION

The following conclusions could be drawn from this study on the analysis of the vibration behaviors of the motor and its optimization.

In this paper, the main vibration harmonic waves of the IPM motor on electric vehicles were investigated by frequency spectrum analysis of the experimental result. It was found that the second, fourth and sixth harmonic waves of the current frequency in the vibration had the highest amplitudes.

The optimization of the radial force based on the parameter sensitivity analysis could result in smaller radial forces without changing the parameters too much. It was also desirable to use the 3-D model of the stator for structural optimization to reduce the dynamic response of the stator.

The final transient dynamic simulation of the optimized model excited by the optimized radial forces showed that the vibration level decreased by 60% averagely, which verified the good effects of the optimization in this paper.

ACKNOWLEDGEMENT

The research was supported by the "973" program of China (2011CB711200) and the National Natural Science Foundation of China (51075302).

REFERENCE

[1] L. C. He, Study on electromagnetic noise of permanent magnet brushless DC drive motor for electric vehicle (in Chinese), Ph.D. Thesis, Tongji University of China, Shanghai, 2012.

[2] Z. Q. Zhu, D. Howe, E. Bolte and B. Achermann, Instantaneous magnetic field distribution in "Brushless permanent magnet DC motors, part I: open-circuit field." *IEEE Trans. Mag.*, vol. 29, no. 1, pp. 124-135, January 1993.

[3] Z. Q. Zhu and D. Howe, "Instantaneous magnetic field distribution in brushless permanent magnet DC motors, part II: armature-reaction field," *IEEE Trans. Mag.*, vol. 29, no. 1, pp. 124-135, January 1993.

[4] Z. Q. Zhu and D. Howe, "Instantaneous magnetic field distribution in brushless permanent magnet DC motors, part III: effect of stator slotting," *IEEE Trans. Mag.*, vol. 29, no. 1, pp. 124-135, January 1993.

[5] Z. Q. Zhu and D. Howe, "Instantaneous magnetic field distribution in brushless permanent magnet DC motors, part IV: magnetic field on load," *IEEE Trans. Mag.*, vol. 29, no. 1, pp. 124-135, January 1993.

[6] H. S. Chen and M. C. Tsai, "Design considerations of electromagnetic force in a direct drive permanent magnet brushless motor," *Journal of Applied Physics*, vol. 103, no. 7, pp. 7F117-1-3, April 2008.

[7] H. J. Zhang, J. J. Zhang and R. Z. Gao, "Radial force reduction for switched reluctance motor with skewed slot structure based on FEM," *Journal of Scientific and Industrial Research*, vol. 69, no. 8, pp. 594-599, August 2010.

[8] "Analytical and FEM based calculation of electromagnetic forces exerted on cylindrical coils due to their own current," *Applied Computational Electromagnetics Society Journal*, vol. 27, no. 11, pp. 866-872, November 2012.

[9] J. S. Choi, K. Izui, S. Nishiwaki, A. Kawamoto and T. Nomura, "Topology optimization of the stator for minimizing gogging torque of IPM motors," *IEEE Trans. Mag.*, vol. 47, no. 10, pp. 3024-3027, October 2011.

[10] J. Kwack, S. Min and J. P. Hong, "Optimal stator design of interior permanent magnet motor to reduce torque ripple using the level set method,"

IEEE Trans. Mag., vol. 46, no. 6, pp. 2108-2111, June 2010.

[11] X. Y. Wang, Q. Y. Wang and Y. F. Wang, "Analysis of the magnetic field of the six-phase disc PMSM and effect of air gap length on the air gap magnetic field," *2008 11th International Conference on Electrical Machines and Systems (ICEMS 2008)*, pp. 3212-3215, 2008.

[12] L. S. Stephens and M. A. Casemore, "Influence of stator slot geometry and rotor eccentricity on field distribution in cylindrical magnetic actuators," *IEEE Trans. Mag.*, vol. 38, no. 2, pp. 1348-1356, March 2002.

[13] D. M. Hamby, "A review of techniques for parameter sensitivity analysis of environmental models," *Environmental Monitoring and Assessment*, vol. 32, no. 2, pp. 135-154, September 1994.

[14] R. F. Chen, Study of vibration and noise characteristics and optimal design of stator of brushless DC drive motor (in Chinese), Master Thesis, Tongji University of China, Shanghai, 2011.

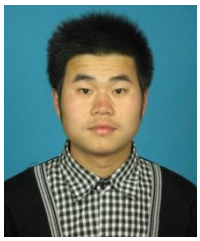

Longyang Xiang a PhD candidate majoring in Vehicle Engineering at Tongji University, Shanghai, China. He received his Bachelor degree of Mechanical Engineering in 2010 from Hunan University, Changsha, China. His main research interests are in the control of vibration and noise of vehicles and analysis and design of mufflers.

Shuguang Zuo a professor at Tongji University, Shanghai, China. He received his B.S. degree in Mechanical Design and Manufacture from Hunan Agricultural University, Changsha, China in 1990 and his M.S. and Ph.D. degrees in Vehicle Engineering from Jilin University, Changchun, China in 1993 and 1996, respectively. He joined Tongji University, Shanghai, China, as Associate Professor in 1998, then he became a professor in 2004. His main research interests are in the control of vibration and noise of vehicles and vehicle system dynamics.